An Internal Model Direct Power Control With Improved Voltage Balancing Strategy for Single-Phase Cascaded H-Bridge Rectifiers

Haoran Liu, Lei Ma, *Member, IEEE*, Wensheng Song, *Member, IEEE*, and Lin Peng

***Abstract*—Single-phase cascaded H-bridge rectifiers (CHBR) are widely studied for vehicular power electronic transformers. In this article, an internal model direct power control (IM-DPC) with a voltage balancing strategy is proposed to improve the control performance of CHBR. First, a modified power control structure is built by the relationship of coordinate transformation. On this basis, the IM-DPC method is presented to obtain a straightforward design for the inner-loop. This approach can be implemented without phase-locked loop, and coordinate transformation is not necessary as well. Then, a first-order transfer function between the difference of dc-side voltage square and that of power is constructed. Further, a novel calculation structure for the compensation duty cycle is proposed. Through the proposed voltage balancing control scheme, the dynamic performance of the dc-side voltage is improved when load unbalancing occurs. The coupling effect between the overall control for the CHBR is also eliminated. Finally, experimental prototype tests are conducted to verify the effectiveness of the proposed method.**

***Index Terms*—Cascaded H-bridge rectifiers (CHBR), direct power control, duty cycle compensation, power electronic transformer (PET), voltage balancing control (VBC).**

I. Introduction

With the rapid development of high-speed railways, high power density, and lightweight turn into the central development tendency of the locomotive traction systems for high-speed electric multiple units (EMUs) [1]. Traditional line frequency transformers fail to meet these requirements due to the low working frequency and bulky mass [2]. Power electronic transformers (PET) are extensively perceived as the momentous equipment to be applied in the next-generation high-speed EMUs thanks to the advantages such as high power density, lightweight, and friendly environment impact [3]. A typical PET traction system is mainly formed by four portions: a single-phase cascaded H-bridge rectifier (CHBR); a bidirectional isolated dc–dc converter; a three-phase inverter; and a traction motor [4]. As the intermediate link of the PET system, the control performance of CHBR is crucial for its stable operation. The control system of CHBR is typically divided into two subsystems, i.e., the dual closed-loop control (outer- and inner-loop) and the voltage balancing control (VBC) [5].

The main objective of the dual closed-loop control is to draw a sinusoidal ac-side current with unity power factor and offer fast dynamic performance [6]. To this end, various approaches have been conducted [6]–[13], [15]. Among them, indirect current control is simple and free of current detection. However, its weak antidisturbance capacity and poor robustness are troublesome problems. [7]. Although hysteresis current control enjoys a quickly dynamic performance, it is hard to design a filter to eliminate broadband harmonics [8]. Nowadays, two control schemes are widely reported in locomotive traction applications, namely the transient direct current control (TDCC) [9] and the proportional-integral-based voltage-oriented control (PI-based VOC) [10]. TDCC is simple to implement with a fast dynamic response speed. However, it comes with a nonzero steady-state error of the ac-side current, which can not assure unity power factor [11]. To address this problem, PI-based VOC transforms the ac variables into dc signals by the coordinate transformation. Then, PI controllers are applied to achieve zero tracking error of the ac-side current [10]. Yet, it suffers from poor dynamic performance [11]. Furthermore, with the PI-based VOC method, the $(N+2)$ times coordinate transformations should be employed to get the total duty cycle for N H-bridge cells system [5]. It will increase calculation burden of the digital signal processor (DSP). Proportional-resonant (PR) control can also eliminate the steady-state error by a large gain at the target (resonant) frequency. However, it is sensitive to the variations in the grid-side frequency [1]. In [12], an adaptation algorithm of the resonant control method is presented, but the choice of parameter is intricate. From the perspective of the control structure, phase information about the grid voltage is necessary for the above control methods [1], [7], [9]–[12]. It can be drawn by the phase-locked loop (PLL). However, it is challenging to realize fast and accurate phase tracking when power quality problems, such as amplitude and frequency variation occur on the grid voltage [13]. Moreover, it is hard and time-consuming to

Manuscript received August 26, 2021; revised December 1, 2021 and January 27, 2022; accepted March 12, 2022. Date of publication March 17, 2022; date of current version April 28, 2022. This work was supported in part by the National Natural Science Foundation of China under Grant 61733015, and in part by the High-Speed Railway Joint Funds of National Natural Science Foundation of China under Grant U1934204. Recommended for publication by Associate Editor M. A. Perez. *(Corresponding author: Lei Ma.)*

Haoran Liu, Lei Ma, and Wensheng Song are with the School of Electrical Engineering, Southwest Jiaotong University, Chengdu 611756, China (e-mail: lhrswjtu@163.com; malei@swjtu.edu.cn; songwengsheng@163.com).

Lin Peng is with the School of Electrical Engineering, Southwest Jiaotong University, Chengdu 611756, China, and also with the Department of Electrical Engineering, Sichuan Engineering Technical College, Deyang 618000, China (e-mail: mildfalchion@126.com).

Color versions of one or more figures in this article are available at https://doi.org/10.1109/TPEL.2022.3160199.

Digital Object Identifier 10.1109/TPEL.2022.3160199

tune the PLL parameters [14]. Therefore, the control system of CHBR without PLL is desirable. Recently, predictive control has attracted much attention for the CHBR system thanks to its fast dynamic response speed. A cell-by-cell-based finite-control-set model predictive control (FCS-MPC) is proposed in [15], and good tracking performance of the ac-side current is obtained. Nevertheless, it cannot avoid the time-consuming tuning of the weight factors to handle multiple control objectives. In short, the aforementioned methods only control the ac-side current, while the power of rectifiers is more concerned than the ac-side current and needs to be controlled directly [6]. Then, a model predictive direct power control (MP-DPC) with the modulation function optimization is applied to the CHBR in [6]. Compared with the cell-by-cell-based FCS-MPC, the proposed MP-DPC is uncorrelated to the weighting factor of the cost function. However, online parameter identification is needed to enhance the system robustness [16], which gives rise to a considerable effort of calculations, so the system complexity also increases [17].

On the other hand, establishing a stable output voltage on the dc-side is the goal of the VBC strategy [15]. Considerable researches have also been done in succession, which can be categorized into two classes. The former is the advanced modulation strategy [18]–[20], such as sorting of the dc-side voltage [18] and the three-dimensional (3-D) space modulation technique [19]. It ensures the voltage balancing on the dc-side, even when there is a significant difference in the load. However, it is difficult to expand these modulation-based methods to the CHBR system with a large number of H-bridge cells [5]. Consequently, lots of researchers are inclined to the latter choice, namely, the duty cycle compensation scheme seeing its easy implementation [5], [9], [12], [21]–[23]. To name a few, the VBC methods with N individual PI controllers are used in [9] and [21], the compensation components are the output of the PI controllers multiplied by the sinusoidal signal of grid voltage and the basic duty cycle, respectively. However, the coupling effect between the dual closed-loop control and the VBC is not considered in both two methods. The coupling effect has an inscrutable influence on the control of the dual closed-loop system, which makes the independent design of the two subsystems for CHBR control impractical [23]. Given this problem, N–1 PI controllers with PI-based VOC technique is used to generate the compensation component of the Nth duty cycle in [22]. Still, the decoupled relationship can only be achieved under the load balancing state. Differently, a new reckoning way with PI-based VOC is provided in [5], and it can completely decouple the two subsystems of the CHBR. However, the dynamic response of voltage balancing is not satisfactory. In reality, the longer settling time of the dc-side voltage under the unbalancing load, the more potential serious damage to the system [1]. Thus, fast dynamic performance of the voltage balancing is imperative for the CHBR system. To strengthen the dynamic performance of voltage balancing, the VBC method based on the dynamic references design concept is revealed in [23]. However, it lacks integral effect, so power compensation is needed. Moreover, the selection of prediction horizon and correction coefficient is a bit complicated. In [12], the VBC method based on energy estimation of each dc-side capacitor bank is presented. Yet, it is essentially a proportional controller with fixed parameters, thus suffering steady-state error.

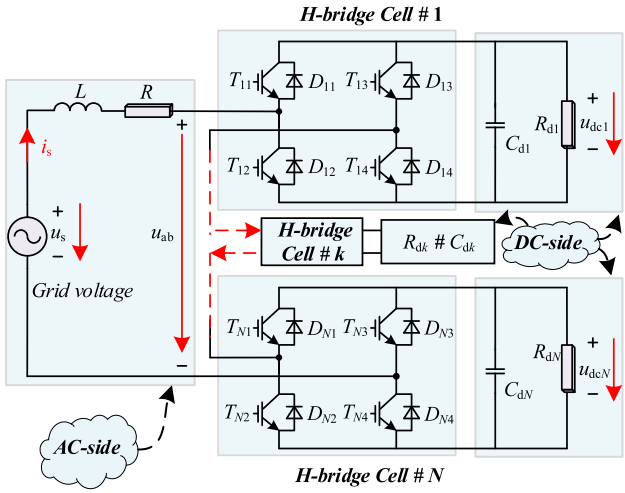

Fig. 1. Topology of a single-phase CHBR.

With a comprehensive consideration of the limitations mentioned above, the motivation of this article is to design a simple control strategy with fast dynamic performance for the CHBR system. An internal model direct power control (IM-DPC) with improved VBC strategy is proposed. The main contributions are enumerated as follows.

1) *Performance Improvement of the Dual Closed-Loop s Control*: Unity power factor can be realized in steady state. In addition, it provides better dynamic performance in the inner-loop and stronger robustness compared with the method in [5].
2) *Performance Improvement of the VBC*: The dynamic response of the voltage balancing by the proposed VBC strategy is enhanced. Besides, there is no coupling effect between the dual closed-loop control and the VBC.
3) *Easy Implementation:* IM-DPC can be applied with a single tuning parameter. Moreover, the PLL and the coordinate transformation are not demanded.

The rest of this article is organized as follows. The mathematic model of the single-phase CHBR is developed in Section II. Then, the modified power control structure and the IM-DPC method are presented in Section III. In Section IV, the improved VBC method is analyzed in detail. The stability analysis of the two subsystems is demonstrated in Section V. Experimental results are exhibited in Section VI. Finally, Section VII concludes this article.

II. Mathematic Model of Single-Phase CHBR

Fig. 1 depicts the topology of a single-phase CHBR with N series-connected H-bridge cells, where each H-bridge cell is constituted by four insulated-gate bipolar transistors (IGBT) T_{k1}-T_{k4} ($k = 1, 2, \ldots N$) with four antiparallel diodes D_{k1}-D_{k4}; u_s denotes the grid voltage; i_s represents the ac-side current; L and R refer to the equivalent inductance and resistance of the adopted CHBR, respectively; C_{dk} and R_{dk} are the dc-side capacitors

and load resistances of the *k*th rectifier cell, respectively; $u_{\mathrm{dc}k}$ represents the *k*th dc-side voltage and can synthesize the total input voltage u_{ab} of the CHBR.

The relationship between the grid voltage and the ac-side current in the $\alpha\beta$ coordinate is available via the following equation [6]

$$\begin{cases} L\frac{di_{s\alpha}}{dt} = u_{s\alpha} - Ri_{s\alpha} - u_{ab\alpha} \\ L\frac{di_{s\beta}}{dt} = u_{s\beta} - Ri_{s\beta} - u_{ab\beta} \end{cases} \tag{1}$$

where $u_{s\alpha}$, $u_{s\beta}$, $i_{s\alpha}$, and $i_{s\beta}$ represent the α-axis and β-axis components of u_s and i_s, respectively; $u_{ab\alpha}$ and $u_{ab\beta}$ denote the α-axis and β-axis components of the input voltage u_{ab}, respectively.

Using the second-order generalized integrator (SOGI) to extract the fundamental component of u_{s} and i_{s} in the $\alpha\beta$ coordinate [16], it leads to

$$\begin{cases} u_{s\alpha} = u_{\mathrm{sm}}\cos(\omega t) = u_s \\ u_{s\beta} = u_{\mathrm{sm}}\sin(\omega t) \end{cases} \tag{2}$$

$$\begin{cases} i_{s\alpha} = i_{\mathrm{sm}}\cos(\omega t - \varphi) = i_s \\ i_{s\beta} = i_{\mathrm{sm}}\sin(\omega t - \varphi) \end{cases} \tag{3}$$

where u_{sm} and i_{sm} represent the peak amplitudes of u_{s} and i_{s}, respectively; φ denotes the phase difference from u_{s} to i_{s}; ω refers to the angular frequency of the fundamental grid voltage, and $\omega = 2\pi f_0$. f_0 represents the fundamental frequency of the grid voltage.

On account of the instantaneous power theory, the active power *P* and the reactive power *Q* of the single-phase CHBR are defined as [24]

$$\begin{cases} P = \frac{u_{\mathrm{sm}}i_{\mathrm{sm}}\cos\varphi}{2} = \frac{u_{s\alpha}i_{s\alpha}+u_{s\beta}i_{s\beta}}{2} \\ Q = \frac{u_{\mathrm{sm}}i_{\mathrm{sm}}\sin\varphi}{2} = \frac{u_{s\beta}i_{s\alpha}-u_{s\alpha}i_{s\beta}}{2}. \end{cases} \tag{4}$$

III. Proposed Internal Model Direct Power Control Strategy

In this section, the modified power control structure and the IM-DPC method are discussed in detail.

A. Modified Direct Power Control Structure

By differentiating *P* and *Q* in (4) with respect to time *t*, it is derived that

$$\begin{cases} \frac{dP}{dt} = \frac{1}{2}(u_{s\alpha}\frac{di_{s\alpha}}{dt} + i_{s\alpha}\frac{\mathrm{d}u_{s\alpha}}{dt} + u_{s\beta}\frac{di_{s\beta}}{dt} + i_{s\beta}\frac{du_{s\beta}}{dt}) \\ \frac{dQ}{dt} = \frac{1}{2}(u_{s\beta}\frac{di_{s\alpha}}{dt} + i_{s\alpha}\frac{\mathrm{d}u_{s\beta}}{dt} - u_{s\alpha}\frac{\mathrm{d}i_{s\beta}}{dt} - i_{s\beta}\frac{du_{s\alpha}}{dt}). \end{cases} \tag{5}$$

Substituting (1) and (2) into (5), it follows that

$$\begin{cases} \frac{dP}{dt} = \frac{{u_{\mathrm{sm}}}^2}{2L} - \frac{RP}{L} - \omega Q - \frac{1}{2L}(u_{s\alpha}u_{ab\alpha} + u_{s\beta}u_{ab\beta}) \\ \frac{dQ}{dt} = \omega P - \frac{RQ}{L} + \frac{1}{2L}(u_{s\alpha}u_{ab\beta} - u_{s\beta}u_{ab\alpha}). \end{cases} \tag{6}$$

Let u_{P} and u_{Q} separately represent the power modulation signals of the active- and the reactive loop. The two power modulation signals can be described as

$$\begin{cases} u_{\mathrm{P}} = u_{s\alpha}\cdot u_{ab\alpha} + u_{s\beta}\cdot u_{ab\beta} \\ u_{\mathrm{Q}} = -u_{s\beta}\cdot u_{ab\alpha} + u_{s\alpha}\cdot u_{ab\beta}. \end{cases} \tag{7}$$

Invoking (6) and (7) yields

$$\begin{cases} \frac{dP}{dt} = \frac{{u_{\mathrm{sm}}}^2}{2L} - \frac{RP}{L} - \omega Q - \frac{1}{2L}u_{\mathrm{P}} \\ \frac{dQ}{dt} = \omega P - \frac{RQ}{L} + \frac{1}{2L}u_{\mathrm{Q}}. \end{cases} \tag{8}$$

Then, by considering (2), (7) can be reorganized as

$$\begin{cases} u_{\mathrm{P}} = u_{\mathrm{sm}}\cos(\omega t)\cdot u_{ab\alpha} + u_{\mathrm{sm}}\sin(\omega t)\cdot u_{ab\beta} \\ u_{\mathrm{Q}} = -u_{\mathrm{sm}}\sin(\omega t)\cdot u_{ab\alpha} + u_{\mathrm{sm}}\cos(\omega t)\cdot u_{ab\beta}. \end{cases} \tag{9}$$

Fortunately, the trigonometric function on the right-hand side of (9) is the transformation from the $\alpha\beta$- to the *dq* coordinates [25].

According to the transformation relationship from the *dq* coordinate to the $\alpha\beta$ coordinate, the following equation is established immediately as

$$\begin{cases} u_{ab\alpha} = \frac{u_{\mathrm{P}}}{u_{\mathrm{sm}}}\cos(\omega t) - \frac{u_{\mathrm{Q}}}{u_{\mathrm{sm}}}\sin(\omega t) \\ u_{ab\beta} = \frac{u_{\mathrm{P}}}{u_{\mathrm{sm}}}\sin(\omega t) + \frac{u_{\mathrm{Q}}}{u_{\mathrm{sm}}}\cos(\omega t). \end{cases} \tag{10}$$

Multiplying the numerator and denominator of the right-hand side in (10) by u_{sm}, and recalling (2), one obtains

$$\begin{cases} u_{ab\alpha} = \frac{u_{s\alpha}u_{\mathrm{P}} - u_{s\beta}u_{\mathrm{Q}}}{{u_{\mathrm{sm}}}^2} \\ u_{ab\beta} = \frac{u_{s\beta}u_{\mathrm{P}} + u_{s\alpha}u_{\mathrm{Q}}}{{u_{\mathrm{sm}}}^2}. \end{cases} \tag{11}$$

From (11), it is clear that u_{P} and u_{Q} must be solved first to figure out $u_{\mathrm{ab}\alpha}$.

Define v_{P} and v_{Q} as the control outputs of the active- and the reactive loop for the modified DPC system, respectively, and it is expressed as

$$\begin{cases} v_P = \frac{{u_{\mathrm{sm}}}^2}{2L} - \omega Q - \frac{1}{2L}u_{\mathrm{P}} \\ v_Q = \omega P + \frac{1}{2L}u_{\mathrm{Q}}. \end{cases} \tag{12}$$

By employing (12), u_{P} and u_{Q} can thus be deduced as

$$\begin{cases} u_{\mathrm{P}} = {u_{\mathrm{sm}}}^2 - 2L(\omega Q + v_P) \\ u_{\mathrm{Q}} = 2L(v_Q - \omega P). \end{cases} \tag{13}$$

Now, v_{P} and v_{Q} are the only unknown variables to find $u_{\mathrm{ab}\alpha}$. Integrating (12) into (8) gives

$$\frac{dP}{dt} = -\frac{R}{L}P + v_P,\ \frac{dQ}{dt} = -\frac{R}{L}Q + v_{\mathrm{Q}} \tag{14}$$

where *P* and *Q* become the state variables, v_{P} and v_{Q} are the input variables of the control system, respectively.

The state-space model and the transfer function of the modified power loop is further shown as

$$\begin{cases} G_{\mathrm{NP}} = G_{\mathrm{NQ}} = \begin{bmatrix} -\frac{R}{L} & 1 \\ 1 & 0 \end{bmatrix} = \begin{bmatrix} A & B \\ C & D \end{bmatrix} \\ G_{\mathrm{NP}}(s) = G_{\mathrm{NQ}}(s) = C(sI - A)^{-1}B + D \end{cases} \tag{15}$$

where G_{NP} and G_{NQ} represent the nominal model (control plant) of the active- and the reactive power loop, respectively.

Control structure of the power closed loop can be depicted in Fig. 2, where e_{P} and e_{Q} are the power difference of the active- and the reactive power loop, respectively; P_{ref} and Q_{ref} represent the power reference of the active- and the reactive power loop; K_P and K_Q refer to the controllers to be designed of the active- and the reactive power loop, respectively.

Obviously, v_{P} and v_{Q} are the outputs of the controller K_P and K_Q in Fig. 2, respectively [26].

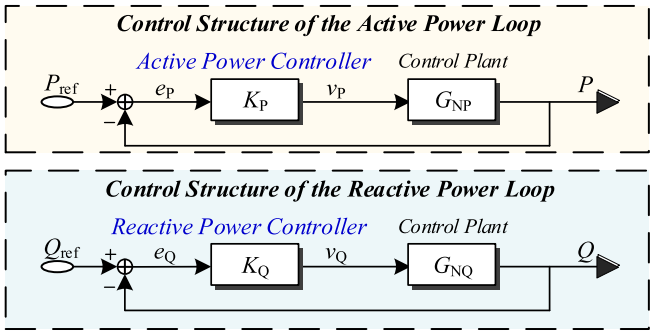

Fig. 2. Block diagram of the power closed-loop control structure.

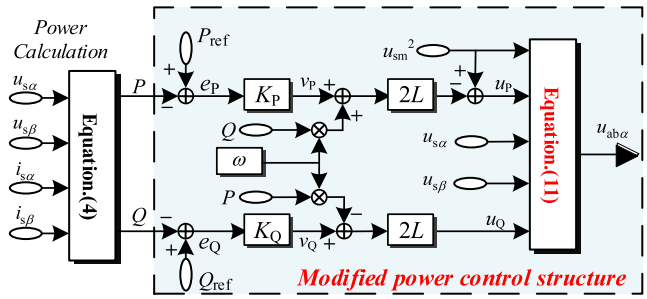

Fig. 3. Block diagram of the modified power control structure.

Fig. 3 shows the control structure of the modified power loop. Compared with the structure of the PI-based VOC [10], [23] and the PI-based DPC [24], the modified DPC structure does not need the coordinate transformation. Moreover, unlike the TDCC and the PR control method in the stationary reference frame, it does not require the phase information of grid voltage to produce the current reference [1], [9]. Thus, the modified DPC structure is irrelative to the PLL. With this modified structure, it can be expected less computational effort.

B. Internal Model Direct Power Control

After establishing the modified power control structure, K_P and K_Q can be designed by the PI control method. However, the two parameters of the PI controller may increase the tuning complexity in the inner-loop [25]. Hence, internal model control (IMC) is applied to provide an alternative solution [27]. IMC method has been successfully researched in permanent magnet synchronous machines [28], turbocharged gasoline engines [29] and induction motors [30] due to its simple structure and less computational burden [31]. However, IMC has seldom been investigated in the inner-loop control of the CHBR for locomotive traction applications. Here, the IMC method based on the modified DPC structure is employed to obtain a straightforward design for the inner-loop control.

The controllers K_P and K_Q are set to be the same to achieve the comparable control effect on the active and the reactive power loops [10]. Moreover, it can be seen from Fig. 2 that the closed-loop control structure of the active and the reactive power is consistent. Therefore, the design process of K_P and

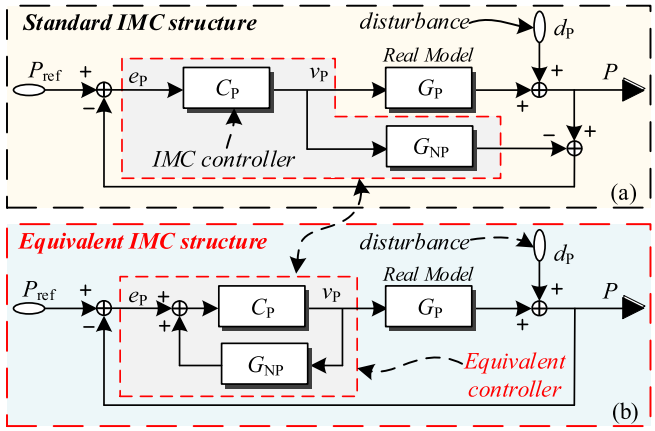

Fig. 4. Block diagram of the IMC structure. (a) Standard IMC structure. (b) Equivalent IMC structure.

K_Q is identical. For ease of presentation, only the controller of active power loop is analyzed in this article.

Fig. 4 exhibits the block diagram of the IMC structure, where G_P refers to the real model of active power loop; C_P represents the IMC controller; and d_P is the external disturbance.

From the standard IMC structure in Fig. 4(a), one is inferred in the Laplace domain that

$$\begin{cases} v_P(s) = \frac{(P_{\text{ref}}(s) - d_P(s)) \cdot C_P(s)}{1 + C_P(s)(G_P(s) - G_{\text{NP}}(s))} \\ P(s) = G_P(s) v_P + d_P(s). \end{cases} \tag{16}$$

Then, (16) can be further rewritten as

$$P(s) = \frac{C_P(s)G_P(s)P_{\text{ref}}(s) + (1 - C_P(s)G_P(s))d_P(s)}{1 + C_P(s)(G_P(s) - G_{\text{NP}}(s))}. \tag{17}$$

Assume that the nominal model is an accurate representation of the real model, it has $G_P(s) = G_{\text{NP}}(s)$. The IMC controller is implemented by the inverse of G_{NP}, i.e., $C_P(s) = G_{\text{NP}}(s)^{-1}$ [27]. Then, it derives that $P(s) = P_{\text{ref}}(s)$. It is indicated that the perfect tracking performance and strong antidisturbance ability are achieved by the IMC method. Unfortunately, this conclusion is hard to realize in practice system because the inverse of G_{NP} may be irrational. To prevent this problem, the IMC controller C_P is designed by introducing a low-pass filter [32]. Since the input of the power loop is a dc signal, the inclusion of the low-pass filter has few effects on the phase delay of the control system. By (15), it follows that

$$C_P(s) = G_{\text{NP}}(s)^{-1} \frac{1}{(\lambda s + 1)^n} = \frac{sL + R}{L(\lambda s + 1)^n} \tag{18}$$

where λ and n represent the filter parameter and the filter order, respectively.

The smaller n is, the simpler the controller can be achieved. The controller $C_P(s)$ in (18) can be realized when $n = 1$. Thus, the filter order n is set as 1 to facilitate the controller implementation in DSP.

To rearrange the standard IMC structure into the equivalent structure in Fig. 4(b), the equivalent active power controller

$K_P(s)$ is formed as

$$K_P(s) = \frac{C_P(s)}{1 - C_P(s)G_{\mathrm{NP}}(s)}. \tag{19}$$

When $G_P(s)$ is not equal to $G_{\mathrm{NP}}(s)$, the perturbation can be depicted by a multiplicative uncertainty model. The sufficient and necessary condition for robust stability of the power system is [30]

$$W_P(s) < |\lambda s + 1| \tag{20}$$

where $W_P(s)$ refers to the multiplicative uncertainty bound.

From (20), it can be deduced that the robustness performance is positively correlated with λ. Moreover, the tracking- and anti-disturbance performance of the power system are also related to λ [32]. Therefore, IM-DPC is convenient in practical locomotive traction applications with a single tuning parameter λ. The selection of λ for the CHBR system will be discussed in Section VI.

IV. Improved Voltage Balancing Control

In this section, the VBC scheme is presented. The purpose of this method is to improve the dynamic performance of voltage balancing on the dc-side from the point of energy balance theory.

Based on the theory of the instantaneous power, the following equation is derived in the $\alpha\beta$ coordinate [23]:

$$\begin{cases} P_{\mathrm{ac}k} = \frac{1}{2}(d_{\alpha k} i_{s\alpha} + d_{\beta k} i_{s\beta}) u_{dck} \\ Q_{\mathrm{ac}k} = \frac{1}{2}(d_{\beta k} i_{s\alpha} - d_{\alpha k} i_{s\beta}) u_{dck} \\ P_{av} = \frac{1}{2}(d_{\alpha} i_{s\alpha} + d_{\beta} i_{s\beta}) u_{dav} \\ Q_{av} = \frac{1}{2}(d_{\beta} i_{s\alpha} - d_{\alpha} i_{s\beta}) u_{dav} \end{cases} \tag{21}$$

where $P_{\mathrm{ac}k}$ and $Q_{\mathrm{ac}k}$ refer to the input instantaneous active power and reactive power for the kth H-bridge cell, respectively; P_{av} and Q_{av} represent the input average active power and reactive power for each H-bridge cell, respectively.

In (21), $d_{\alpha k}$ and $d_{\beta k}$ are the total duty cycle of the α- axis and the β-axis for the kth H-bridge cell; d_α and d_β stand for the basic duty cycle of the α-axis and the β-axis, respectively; $\Delta_{\alpha k}$ and $\Delta_{\beta k}$ are the compensation duty cycles of the kth H-bridge cell that help to keep the voltage balancing on the dc-side when load unbalancing occurs; u_{dav} represents the average voltage of the dc-side. These variables are given by

$$\begin{cases} d_{\alpha k} = d_\alpha + \Delta_{\alpha k} = \frac{u_{ab\alpha}}{N u_{dav}} + \Delta_{\alpha k} \\ d_{\beta k} = d_\beta + \Delta_{\beta k} = \frac{u_{ab\beta}}{N u_{dav}} + \Delta_{\beta k} \\ u_{dav} = \frac{1}{N} \sum_{k=1}^{N} u_{\mathrm{dc}k}. \end{cases} \tag{22}$$

It is supposed that voltage balancing on the dc-side can be achieved by the proposed VBC, i.e., $u_{\mathrm{dc}k} = u_{dav}$, and relying on (21) results in

$$P_{\Delta k} = P_{\mathrm{ac}k} - P_{av} = \frac{1}{2}(\Delta_{\alpha k} \cdot i_{s\alpha} + \Delta_{\beta k} \cdot i_{s\beta}) \cdot u_{\mathrm{dc}k} \tag{23}$$

where $P_{\Delta k}$ represents the difference between $P_{\mathrm{ac}k}$ and P_{av}.

Additionally, recalling (21) leads to

$$Q_{\Delta k} = Q_{\mathrm{ac}k} - Q_{av} = \tfrac{1}{2} \cdot (d_{\beta k} i_{s\alpha} - d_{\alpha k} i_{s\beta})(u_{dck} - u_{dav}) + \tfrac{1}{2} \cdot (\Delta_{\beta k} \cdot i_{s\alpha} - \Delta_{\alpha k} \cdot i_{s\beta}) \cdot u_{\mathrm{dc}k} \tag{24}$$

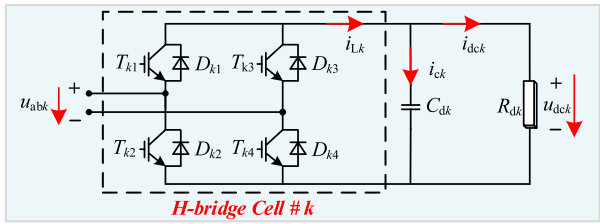

Fig. 5. Equivalent circuit of the kth H-bridge cell.

where $Q_{\Delta k}$ represents the difference between $Q_{\mathrm{ac}k}$ and Q_{av}.

As can be observed from (24), the compensation duty cycle will affect the reactive power in spite of that $u_{\mathrm{dc}k} = u_{\mathrm{dav}}$ is attained. For the sake of reactive power balancing, the following equation must be satisfied

$$\Delta_{\beta k} \cdot i_{s\alpha} - \Delta_{\alpha k} \cdot i_{s\beta} = 0, (k = 1, 2, \ldots N). \tag{25}$$

By virtue of (23) and (25) yields

$$\Delta_{\alpha k} = \frac{2 i_{s\alpha}}{{i_{s\alpha}}^2 + {i_{s\beta}}^2} \cdot \frac{P_{\Delta k}}{u_{\mathrm{dc}k}}, (k = 1, 2, \ldots, N). \tag{26}$$

Fig. 5 shows the equivalent circuit of the kth H-bridge cell, where $i_{\mathrm{dc}k}$, i_{Lk}, and i_{ck} refer to the load current, dc-side current and capacitor current of the kth H-bridge cell, respectively.

Neglecting the power losses of switches, in line with the energy balance theory, the dynamic equation of the dc-side capacitor, in Fig. 5, is given by [33]

$$\frac{1}{2} C_{dk} \frac{\mathrm{d}{u_{\mathrm{dc}k}}^2}{\mathrm{d}t} = P_{ack} - u_{\mathrm{dc}k} i_{\mathrm{dc}k} = P_{ack} - \frac{{u_{\mathrm{dc}k}}^2}{R_{dk}}. \tag{27}$$

Defining $e_{\mathrm{dc}k} = {u_{\mathrm{dc}k}}^2 - {u_{dav}}^2$, and it derives through invoking (23) and (27) that

$$\begin{aligned} \frac{\mathrm{d}e_{\mathrm{dc}k}}{dt} &= 2 \cdot \left[\frac{(P_{\mathrm{ac}k} - P_{av})}{C_{dk}} - \frac{e_{\mathrm{dc}k}}{R_{dk} \cdot C_{dk}} \right] \\ &= 2 \cdot \left(\frac{P_{\Delta k}}{C_{dk}} - \frac{e_{\mathrm{dc}k}}{R_{dk} \cdot C_{dk}} \right). \end{aligned} \tag{28}$$

Rearranging (28) in the Laplace domain gives

$$G_V(s) = \frac{e_{\mathrm{dc}k}(s)}{P_{\Delta k}(s)} = \frac{R_{dk}}{1 + 0.5 \cdot R_{dk} \cdot s} \tag{29}$$

where $G_V(s)$ is named as the transfer function of the proposed voltage balancing system.

It can be known from (29) that the difference between ${u_{\mathrm{dav}}}^2$ and ${u_{\mathrm{dc}k}}^2$, i.e., $e_{\mathrm{dc}k}$, behaves as a first-order transfer function with $P_{\Delta k}$. Similar to the control structure of PI-based VOC in [26], PI controller can be used to track the system reference, and the input and output of the PI controller are $e_{\mathrm{dc}k}$ and $P_{\Delta k}$, respectively. It should be pointed out that the purpose of (28) is to establish the transfer function relationship between $e_{\mathrm{dc}k}$ and $P_{\Delta k}$. In fact, an approximation is made in (28), i.e., $R_{dk} = R_{av}$, where R_{av} is a virtual average resistance. Although the difference between R_{dk} and R_{av} exists under unbalancing load, the influence on the voltage balancing caused by the difference can be regarded as the disturbance on the control output of the VBC system, and can be diminished by tuning the PI parameters.

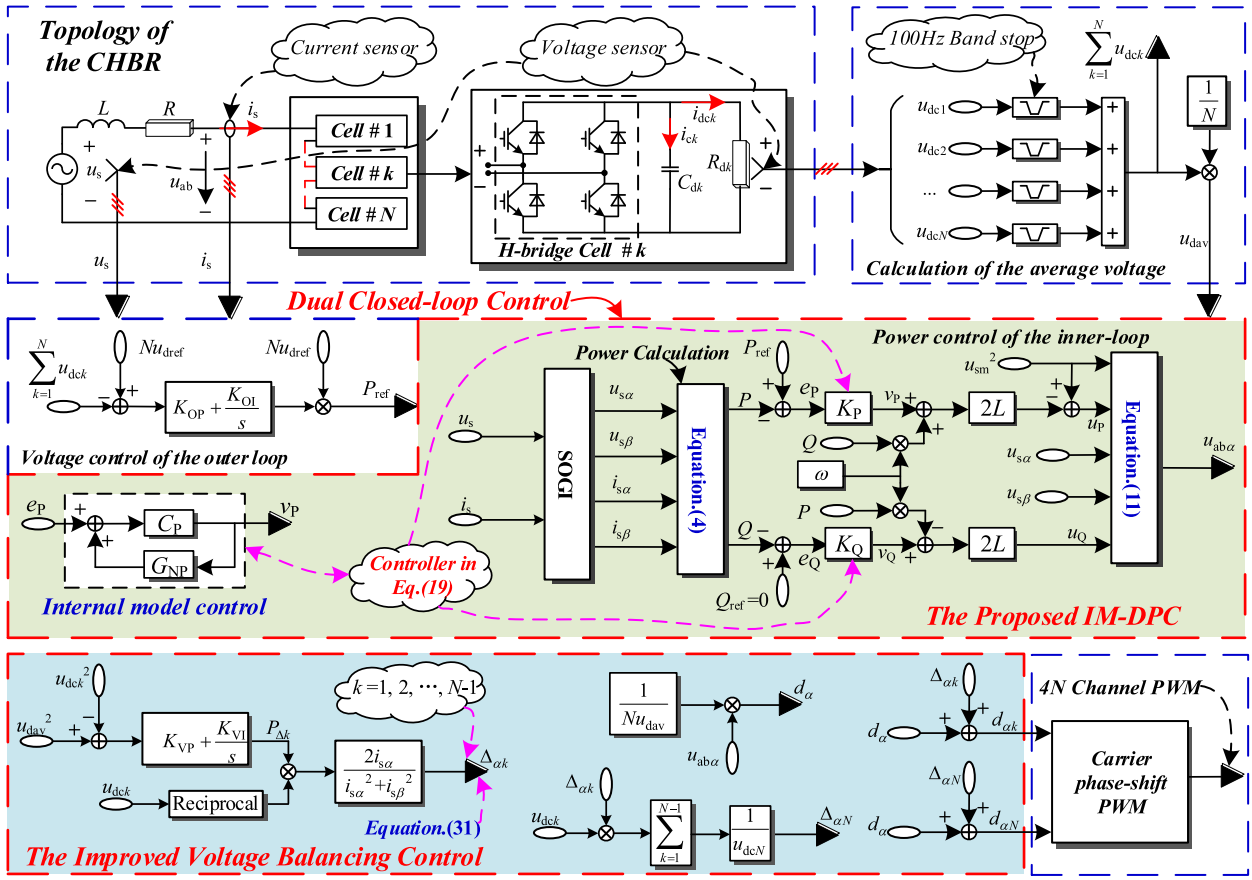

Fig. 6. Block diagram of the proposed IM-DPC with improved VBC strategy.

Eventually, the duty cycle $d_{\alpha k}$ is obtained by substituting $P_{\Delta k}$ into (22) and (26). However, applying (26) to the VBC directly will bring about the coupling effect between the dual closed-loop control and the VBC. In consideration of the coupling index in the dq coordinate, the relationship in the $\alpha\beta$ coordinate is defined as [23]

$$J_\alpha = \left(\sum_{k=1}^{N} \Delta_{\alpha k} u_{\mathrm{dc}k} \right)^2. \tag{30}$$

To minimize the coupling effect of the two subsystems, the expression of the compensation duty cycle $\Delta_{\alpha k}$ in (26) is modified as

$$\begin{cases} \Delta_{\alpha k} = \frac{2 i_{s\alpha}}{{i_{s\alpha}}^2 + {i_{s\beta}}^2} \cdot \frac{P_{\Delta k}}{u_{\mathrm{dc}k}}, (k = 1, 2, \ldots, N-1) \\ \Delta_{\alpha N} = -\frac{1}{u_{\mathrm{dc}N}} \left(\sum_{k=1}^{N-1} \Delta_{\alpha k} u_{\mathrm{dc}k} \right). \end{cases} \tag{31}$$

It can be noticed that the compensation duty cycle $\Delta_{\alpha k}$ is drawn support from $\Delta_{\beta k}$. However, the expression of $\Delta_{\alpha k}$ is out of touch with $\Delta_{\beta k}$ in (31). The reason is that the coordinate transformation is unnecessary for the modified DPC structure, so $\Delta_{\alpha k}$ is added to d_α straightly.

To satisfy the limitation of the modulation index, the total duty cycle should be constrained as [5]

$$d_{\alpha k} = d_\alpha + \Delta_{\alpha k} < 1, (k = 1, 2, \ldots, N). \tag{32}$$

The block diagram of the proposed IM-DPC with improved VBC strategy for the adopted CHBR is demonstrated in Fig. 6, where $d_{\alpha k}$ is used as the input of the phase-shifted PWM (PS-PWM). 100Hz band-stop filters are applied to reduce the second-order harmonic of the dc-side voltages. Q_{ref} is zero for unity power factor operation [6]. To obtain an outstanding performance of SOGI, the damping factor K_{SOGI} of SOGI is set to 1.57 ([16] and [34]).

Unlike the conventional VBC method [5], [9], [21], [22], the proposed VBC method takes the difference $e_{\mathrm{dc}k}$ as the input of the PI controller instead of the difference of dc-side voltage. Moreover, the compensation duty cycle is not generated by the output of the PI controller, whereas it is produced by (31). Since the mathematical model between $e_{\mathrm{dc}k}$ and $P_{\Delta k}$ is constructed by the power theory in this article, a feedback control loop is established to track $e_{\mathrm{dc}k}$. Compared with the VBC approach in [12], the steady-state error of dc-side voltage can be decreased by the proposed feedback system. With this method, it can expect an improved dynamic performance of voltage balancing on the dc-side.

V. Stability Analysis

If the coupling effect is eliminated by the proposed VBC strategy, the stability of the two subsystems can be analyzed independently [5]. This section researches the stability of the of the CHBR control system.

A. Stability of the Dual Closed-Loop Control

The transfer function of the power closed-loop system $G_{\mathrm{CP}}(s)$ is calculated by invoking (15), (18) and (19), it has

$$G_{\mathrm{CP}}(s) = \frac{1}{\lambda s + 1}. \tag{33}$$

Subsequently, it is feasible to construct the characteristic polynomial of $G_{\mathrm{CP}}(s)$ as

$$\lambda s + 1 = 0. \tag{34}$$

In light of the Routh stability criterion, the condition of the power inner-loop system stability is $\lambda > 0$.

From Fig. 5, it is deduced that

$$\frac{u_{\mathrm{dc}k}}{i_{Lk}} = \frac{R_{dk}}{sC_{dk}R_{dk} + 1}. \tag{35}$$

Then, it derives

$$u_{\mathrm{dc}k} = \frac{P_{\mathrm{ac}k}}{u_{\mathrm{dc}k}} \cdot \frac{R_{dk}}{sC_{dk}R_{dk} + 1}. \tag{36}$$

Similar to (36), one obtains

$$\sum_{k=1}^{N} u_{\mathrm{dc}k} = \frac{P}{\sum\limits_{k=1}^{N} u_{\mathrm{dc}k}} \cdot \frac{R_{dk}}{sC_{dk}R_{dk} + 1}. \tag{37}$$

The system control cycle is much less than the grid voltage cycle, so the sample delay can be ignored in the stability analysis. Combing (37) and Fig. 6, the transfer function of the open-loop system for the dual closed-loop $G_{\mathrm{OD}}(s)$ is given by

$$G_{\mathrm{OD}}(s) = K_O(s) \cdot N u_{\mathrm{dref}} \cdot \frac{G_{\mathrm{CP}}(s)}{\sum\limits_{k=1}^{N} u_{\mathrm{dc}k}} \cdot \frac{R_{dk}}{sC_{dk}R_{dk} + 1} \tag{38}$$

where $K_O(s)$ refers to the outer-loop voltage controller.

The transfer function of the closed-loop system $G_{\mathrm{CD}}(s)$ can be expressed as

$$G_{CD}(s) = \frac{K_O(s) \cdot N u_{\mathrm{dref}} \cdot G_{\mathrm{CP}}(s) \cdot R_{dk}}{\sum\limits_{k=1}^{N} u_{\mathrm{dc}k}(sC_{dk}R_{dk} + 1) + K_O(s) \cdot N u_{\mathrm{dref}} \cdot G_{CP}(s) \cdot R_{dk}}. \tag{39}$$

With the expression of $G_{\mathrm{CP}}(s)$ in (33), the characteristic polynomial of $G_{\mathrm{CD}}(s)$ is

$$\sum_{k=1}^{N} u_{dck}\lambda C_{dk}R_{dk}s^3 + \sum_{k=1}^{N} u_{dck}(\lambda + C_{dk}R_{dk})s^2 + \left(\sum_{k=1}^{N} u_{dck} + K_{\mathrm{OP}}R_{dk}N u_{\mathrm{dref}}\right)s + K_{\mathrm{OI}}R_{dk}N u_{\mathrm{dref}} = 0 \tag{40}$$

where K_{OP} and K_{OI} represent the proportional and integral parameters of $K_O(s)$, respectively.

Usually, the parameters of PI controller are designed as positive numbers and $\lambda > 0$, $C_{dk} > 0$, $R_{dk} > 0$. Therefore, the exponential stability of the dual closed-loop system is obtained by the Routh stability criterion.

B. Stability of the VBC

By a standard control structure, one can get

$$G_{CV}(s) = \frac{G_V(s) \cdot K_V(s)}{1 + G_V(s) \cdot K_V(s)} \tag{41}$$

where $G_{CV}(s)$ refers to transfer function of the voltage balancing closed-loop system. $K_V(s)$ is the PI controller of the VBC, and let K_{VP} and K_{VI} represent the proportional and integral parameters of $K_V(s)$, respectively.

Rewrite (41) with (29) leads to

$$G_{CV}(s) = \frac{R_{dk}K_{\mathrm{VP}} \cdot s + R_{dk}K_{\mathrm{VI}}}{0.5 \cdot R_{dk}C_{dk} \cdot s^2 + (R_{dk}K_{\mathrm{VP}} + 1) \cdot s + R_{dk}K_{\mathrm{VI}}}. \tag{42}$$

Accordingly, the characteristic polynomial of $G_{\mathrm{CV}}(s)$ is shown as

$$0.5 \cdot R_{dk}C_{dk} \cdot s^2 + (R_{dk}K_{\mathrm{VP}} + 1)s + R_{dk}K_{\mathrm{VI}} = 0. \tag{43}$$

Therefore, the exponential stability of the VBC system is also guaranteed by the proposed method.

VI. Experiment Verifications

A. Description of the Experimental System

To confirm the effectiveness of the proposed IM-DPC and the VBC strategy, a physical test platform for single-phase CHBR is performed. Three separate H-bridge cells with IGBT (FF200R12KT4) are connected in series to construct the adopted CHBR. The experimental prototype is exhibited in Fig. 7. A 32-bit floating TMS320F28335 DSP board is employed to program the control algorithm in the CCS10.2 environment. The grid voltage is supplied by a 5 kW autotransformer. The A622 current clamp and the 25 MHz/1300 V differential probe are used to measure the waveforms of current and voltage, respectively. A 12 kW electronic load is exploited to change the load resistance. The experimental values of the adopted CHBR are given in Table I [35].

As is well known, the wider the bandwidth of the closed-loop control system, the better corresponding dynamic performance can be [36]. However, the increase in the bandwidth will lead to growth in the overshoot. On the other hand, the pulsewidth modulation (PWM) equivalent switching frequency of the CHBR

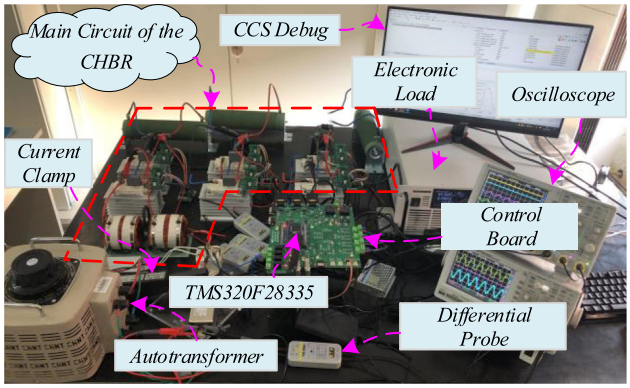

Fig. 7. Experimental prototype of the three-cells single-phase CHBR.

TABLE I
PARAMETERS OF THE CHBR SYSTEM

Parameters	Experimental value
Grid voltage RMS value (u_s)	90V
Grid voltage fundamental frequency (f_0)	50 Hz
AC-side equivalent inductance (L)	5.6mH
AC-side equivalent resistance (R)	0.1Ω
DC-side capacitance (C_{dk})	3.3mF
DC-side load resistance (R_{dk})	20Ω
DC-side reference voltage (u_{dref})	50V
Switching frequency (f_{pwm})	1000Hz
Control cycle (T_c)	50us
Damping factor (K_{SOGI})	1.57
Proportional parameters (K_{OP})	1.0
Integral parameters (K_{OI})	8.0
Proportional parameters (K_{VP})	2.0
Integral parameters (K_{VI})	10.0
Number of H-bridges (N)	3

system can be expressed as Nf_{pwm}, and the higher-order harmonic content of the ac-side current is distributed near $2Nf_{pwm}$ [23]. As can be observed from (4), the instantaneous power includes the component of ac-side current. The increase of the system bandwidth also weakens the suppression ability of high-order harmonic components of the ac-side current. Therefore, the system bandwidth of the power loop is set to be no more than $2Nf_{pwm}$, considering the overshoot of the control system and the suppression of the high-order harmonics of the ac-side current.

With the parameters in Table I, the relationship between the bandwidth of the power closed-loop and the filter parameter λ is shown in Fig. 8. When the switching frequency of the experimental system is 1000 Hz, the bandwidth of the power system should be less than 6000 Hz. Thus, as shown in Fig. 8, the range of λ is $\lambda > 2.66\times10^{-5}$. After the verification by the experimental platform, λ is selected as 1.55×10^{-4}. Then, the

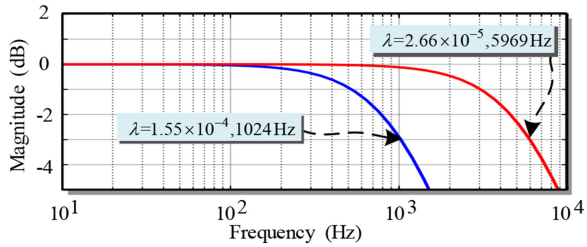

Fig. 8. Relationship between the bandwidth of power closed-loop and the filter parameter λ.

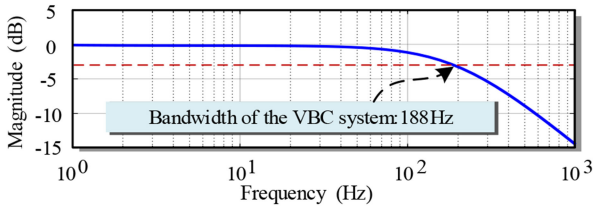

Fig. 9. Magnitude of the VBC system with the parameters in Table I.

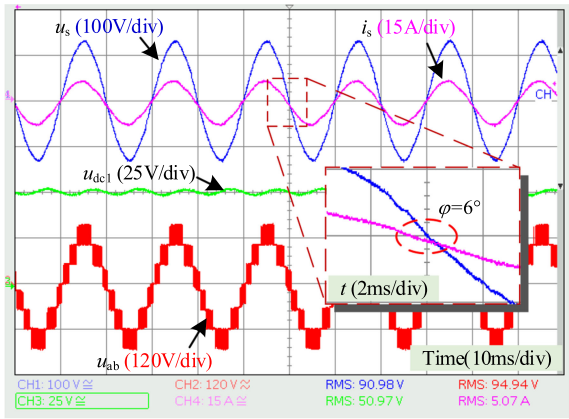

Fig. 10. Experiment results in steady state with the balancing load. (a) TDCC+ the VBC method in [21]. (b) IM-DPC+the proposed VBC method.

TABLE II
EXPERIMENTAL RESULTS OF THE FIVE METHODS WHEN THE LOAD SUDDEN CHANGES

Performance	TDCC+ the VBC method in [21]	PI-based VOC + the VBC method in [5]	PR+ the VBC method in [9]	PR+ the VBC method in [12]	IM-DPC+ the proposed VBC method
Settling time under R_{d2} change	540ms	590ms	455ms	exist steady-state error	71ms
Voltage fluctuation under R_{d2} change	17V	20V	16V	11V	6.5V
Settling time under R_{d3} change	550ms	700ms	420ms	exist steady-state error	64ms
Voltage fluctuation under R_{d3} change	15V	20V	14V	10V	7V

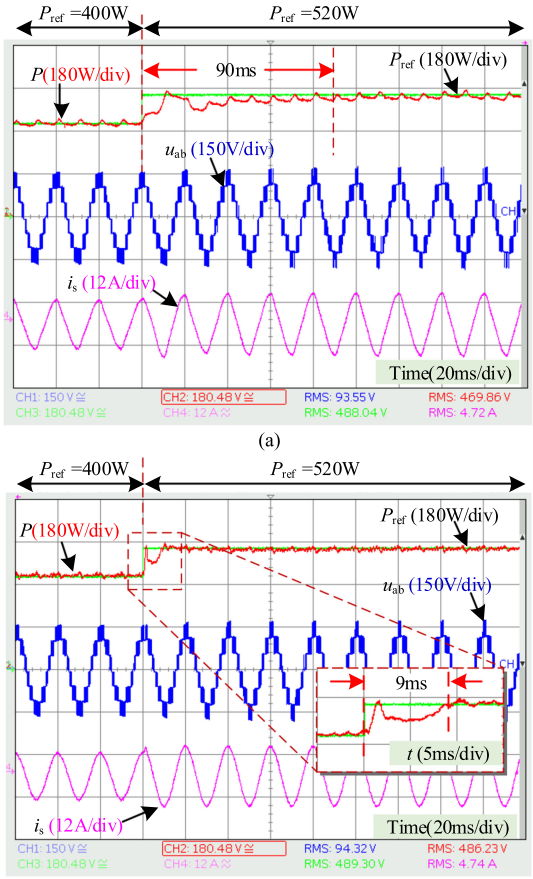

Fig. 11. Experiment results when P_{ref} steps from 400 to 520 W with the balancing load. (a) PI-based VOC. (b) Proposed IM-DPC.

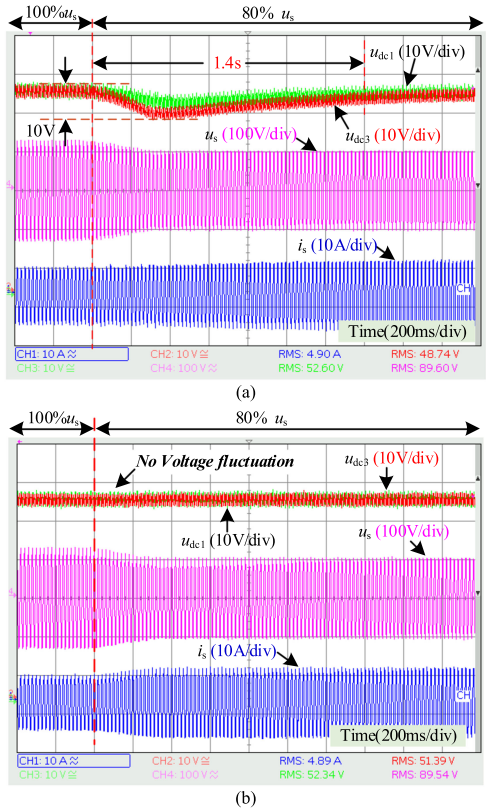

Fig. 12. Experimental results when the amplitude of the grid voltage reduces from 100% to 80%. (a) PI-based VOC+ the VBC method in [5]. (b) IM-DPC+ the proposed VBC method.

power controller is solved by (15), (18), and (19). Due to length limitations, the discretization process of the power controller for DSP is not given, and for more details please refer to [37].

For a single-phase rectifier system, the dc-side voltage contains a fluctuating component with a frequency of $2f_0$ [38]. As can be seen from Fig. 6, the input of the VBC system is ${u_{\rm dav}}^2$, so the $4f_0$ fluctuating component will enter the VBC system. It may increase the fluctuation of the compensation duty cycle and even deteriorate the ac-side current quality. To reduce this impact, let the closed-loop bandwidth of the VBC system be less than $4f_0$. Fig. 9 shows the magnitude of the VBC system with the parameters in Table I. Clearly, the resulting bandwidth is within the set range.

B. Experimental Results

The first test is carried out to assess the performance of the proposed method in steady state with the balancing load. For comparison, the TDCC+ the VBC method in [21], which is widely applied in locomotive traction applications, are tested under identical condition. Fig. 10 demonstrates the experimental results in steady state, where three 20 Ω load resistors are connected in each dc-side. As can be clearly appreciated in Fig. 10, the seven-level voltage u_{ab} are generated by the two control methods, all the ac-side currents emerge nearly sinusoidal waveform, and the dc-side voltages remain close to the reference value. However, the ac-side current in phase with the grid voltage is only realized by the IM-DPC method. With the TDCC method, the phase difference φ between the grid voltage and the ac-side current is 6.0° in Fig. 10(a). This fact is caused

TABLE III
COMPARISON RESULTS OF THE FIVE METHODS

Performance and structure	TDCC+ the VBC method in [21]	PI-based VOC + the VBC method in [5]	PR+ the VBC method in [9]	PR+ the VBC method in [12]	IM-DPC+ the proposed VBC method
PLL	Need	Need	Need	Need	No
Coordinate transformation	No	Need	No	No	No
Unity power factor	No	Yes	Yes	Yes	Yes
Dynamic performance of the inner-loop	Fast	Slow	Fast	Fast	Fast
Coupling effect	Not consider	Decoupled	Not consider	Not consider	Decoupled
Dynamic performance of the VBC	Slow	Slow	Slow	exist steady-state error	Fast
Computation burden	11.8us	21.1us	14.04us	13.6us	12.8us

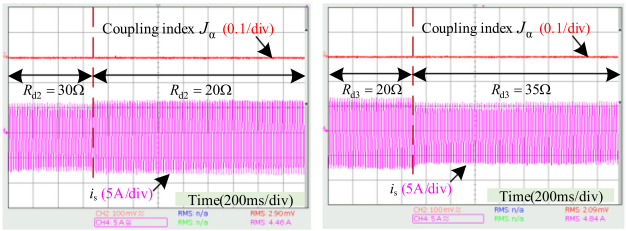

(a) (b)

Fig. 13. Coupling index J_α of the proposed IM-DPC with the improved VBC strategy. (a) R_{d2} steps from 30 to 20 Ω and $R_{d1}=R_{d3}=20$ Ω. (b) R_{d3} steps from 20 to 35 Ω and $R_{d1}=R_{d2}=20$ Ω.

by the PI controller cannot accurately track the 50 Hz current via a finite loop gain [11]. Hence, it can be concluded that the unity power factor can be achieved by the proposed IM-DPC method in steady state.

The second investigation demonstrates the dynamic performance of the proposed IM-DPC method under the active power reference sudden change with the balancing load. For a fair comparison of the dynamic performance, the outer-loop control and the VBC are disconnected. Fig. 11 shows the experimental waveforms when $P_{\rm ref}$ steps up from 400 to 520 W. Once a sudden active reference power changes, as described in Fig. 11(a), the PI-based VOC approach takes about 90 ms to adjust the active power reaching the steady-state again, whereas the settling time of active power by the IM-DPC scheme is about 9ms in Fig. 11(b). In this test, the comparison results confirm that the dynamic performance of the IM-DPC scheme is better than the PI-based VOC strategy.

The grid voltage variation test has been performed to verify the robustness of the proposed control strategy. The experimental results are depicted in Fig. 12, where the grid voltage amplitude is reduced to 80% of the rating value. It should be noted that the change of the grid voltage is realized by the autotransformer, so the voltage change has a regulation process of about 100 ms. Fig. 12 shows the dc-side voltage is close to the reference value under the 100% $u_{\rm s}$, with the PI-based VOC+ the VBC method in [5] and the IM-DPC+ the proposed VBC strategy. However, when the grid voltage dips by 20%, the voltage $u_{\rm dc1}$ and $u_{\rm dc3}$ can not retain in the stable state by the PI-based VOC+ the VBC method in [5], and the voltage fluctuation amplitude of $u_{\rm dc3}$ is 10V. Additionally, the two dc-side voltages take almost 1.4 s to return to their reference value. By comparison, it can be noted from Fig. 12(b) that the change of the grid voltage has no effect on the dc-side voltage by the proposed method. Consequently, it is concluded that the proposed method has stronger robustness against the grid voltage variations.

To exhibit the coupling effect between the dual closed-loop control and the VBC scheme, Fig. 13 illustrates the experimental results of the coupling index J_α by the IM-DPC method with the improved VBC strategy. It is known from [5] and [23] that if the coupling index equals zero under the unbalancing load conditions, the coupling effect is eliminated. Here, it can be observed from Fig. 13 that the coupling index J_α maintained at zero before and after the load R_{d2} or R_{d3} changes. From the experimental results of Fig. 13, one can be concluded that the coupling effect between the two subsystems is get rid of by the proposed control method under both steady state and transient conditions.

Voltage unbalance on the dc-side is the main weakness of the adopted CHBR for the load unbalancing [13]. The final test is provided to demonstrate the dynamic performance of the voltage balance. Fig. 14 explicates the experimental results of the load resistance R_{d2} sudden changes from 20 to 35 Ω, while R_{d1} and R_{d3} retain the nominal value of 20 Ω. As can be seen in Fig. 14(a), the dc-side voltages without the VBC method are maintained at the desired value of 50 V in the beginning. However, after the load resistance changes, the voltage $u_{\rm dc2}$ is about 28 V higher than the voltage $u_{\rm dc1}$ and $u_{\rm dc3}$. The compensation duty cycle of the third load R_{d3} is produced by that of the other two loads, so the experimental test is also conducted when the load R_{d3} sudden changes from 20 to 35 Ω, which is shown in Fig. 15. Table II illustrates the experimental results of Figs. 14 and 15. Clearly, the settling times of the dc-side voltage by the proposed VBC strategy are less than the other four VBC methods when the load R_{d2} or R_{d3} sudden changes. Moreover, the smallest voltage fluctuations of the dc-side voltage are obtained by this method. Therefore, compared with the VBC method in [5], [9], [12], and [21], the improved dynamic performance of the voltage balancing is achieved by the proposed VBC approach.

By (24) and (25), it can be concluded that: the difference $Q_{\Delta k}$ is proportional to the difference between $u_{{\rm dc}k}$ and $u_{\rm dav}$. If the dc-side voltage is in a balancing state, then the reactive power is in balance. From the experimental results of Figs. 14 and 15, the three dc-side voltages are close to the reference value under unbalancing load. As a result, the proposed VBC method has the potential for reactive power balancing.

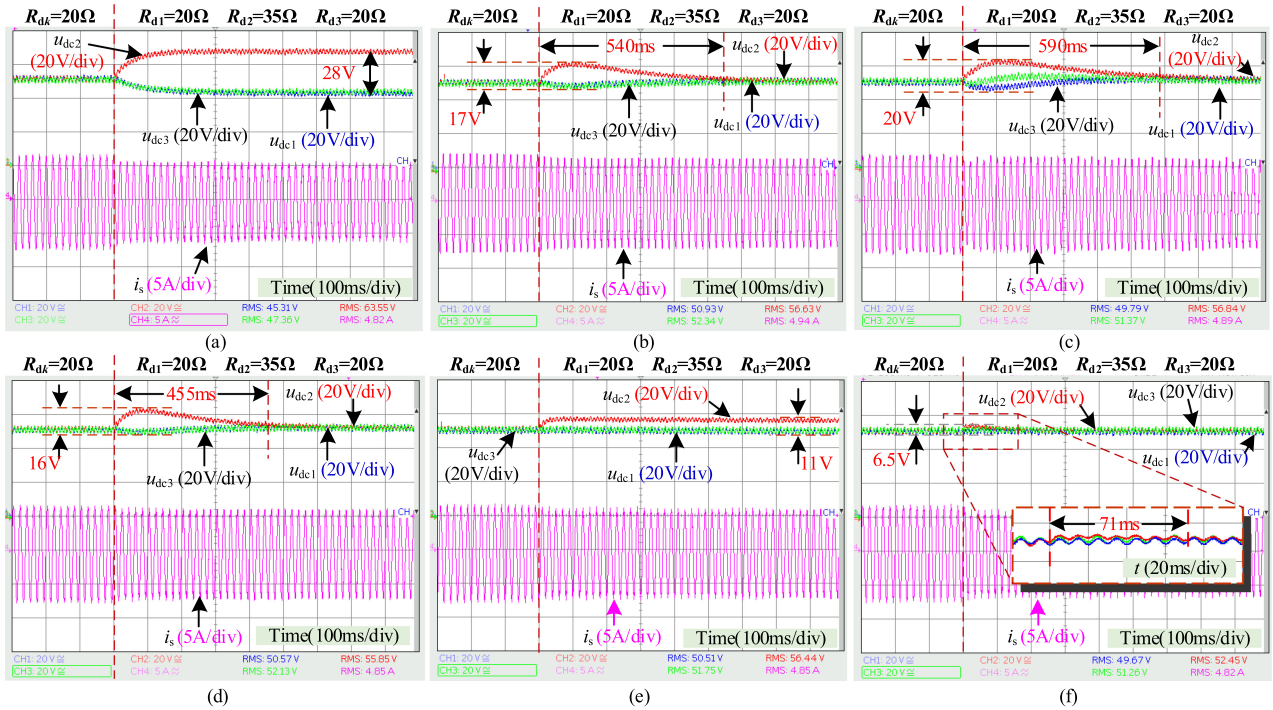

Fig. 14. Experimental results of the dc-side voltages when the load R_{d2} sudden change from 20 to 35Ω. (a) IM-DPC without the VBC method. (b) TDCC+ the VBC method in [21]. (c) PI-based VOC+ the VBC method in [5]. (d) PR control+ the VBC method in [9]. (e) PR control+ the VBC method in [12]. (f) IM-DPC+ the proposed VBC method.

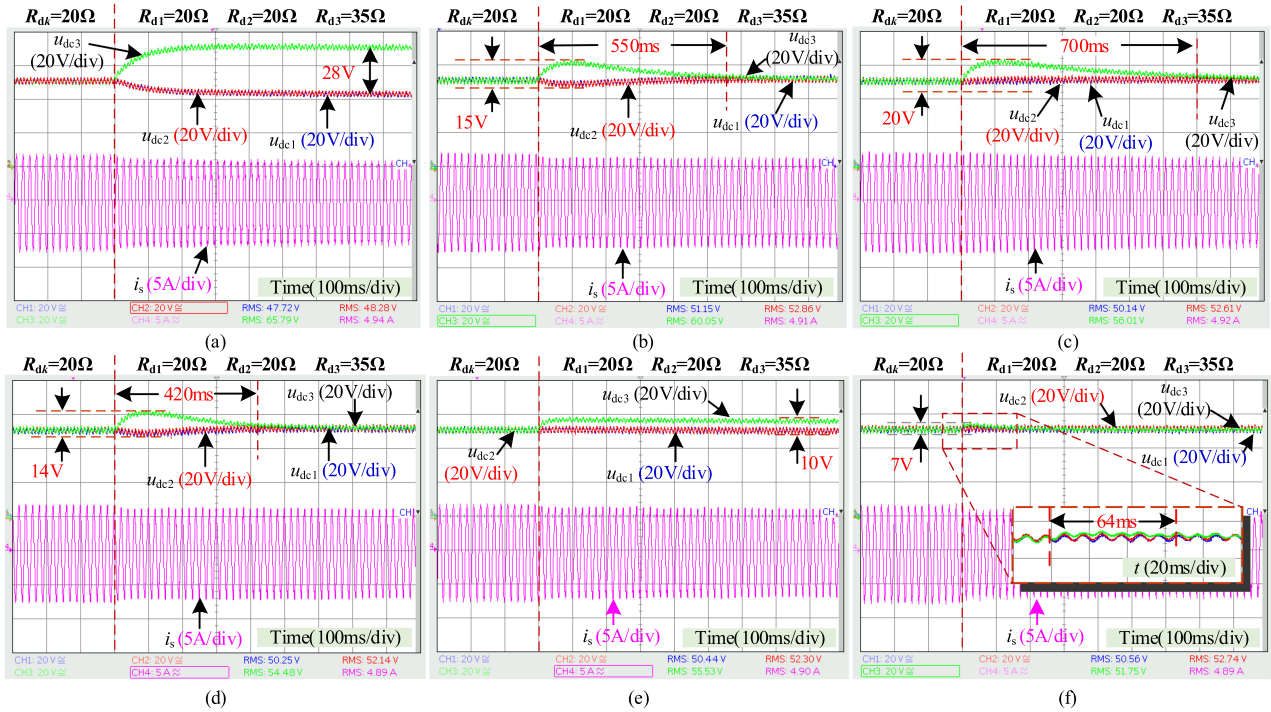

Fig. 15. Experimental results of the dc-side voltages when the load R_{d3} sudden change from 20 to 35Ω. (a) IM-DPC without the VBC method. (b) TDCC+ the VBC method in [21]. (c) PI-based VOC+ the VBC method in [5]. (d) PR control+ the VBC method in [9]. (e) PR control+ the VBC method in [12]. (f) IM-DPC+the proposed VBC method.

Through the above experimental tests, Table III gives the comparison results of the performance and structure for the five methods. The specific algorithm computation burden of the five methods is also given in Table III. Unsurprisingly, the highest computation burden takes place in the PI-based VOC+ the VBC method in [5], because the PI-based VOC method demands the coordinate transformation and PLL. Compared with the TDCC+ the VBC method in [21], the execution time of the proposed control scheme is slightly increased due to the power calculation. However, the unity power factor is assured by the proposed control method, which is significant for the locomotive traction with high power.

VII. Conclusion

In this article, an IM-DPC method with improved VBC strategy was proposed for CHBR in locomotive traction applications. According to the relationship of the coordinate transformation, a modified DPC control structure was constructed without the PLL and the coordinate transformation. Then, the IM-DPC method is developed to achieve a straightforward design with a single tuning parameter. Furthermore, the transfer function relationship between the difference of dc-side voltage square and that of power is obtained. Based on this, a feedback control loop is constructed to keep voltage balancing on the dc-side. The experimental results confirmed that the proposed strategy has the salient features as follows.

1) Different from the control method with the TDCC, it can achieve unity power factor in the steady state.
2) It can provide better dynamic performance and stronger robustness compared with the control method in [5].
3) The dynamic performance of the voltage balancing on the dc-side is improved compared with the VBC method in [5], [9], [12], and [21].
4) No coupling effect exists between the two subsystems of the CHBR.

In addition, since it can be easily implemented, the proposed control strategy is also desirable to single-phase cascaded H-bridge converter-based static synchronous compensator and multilevel active power filter.

References

[1] J. Liu, J. Yang, J. Zhang, Z. Nan, and Q. Zheng, "Voltage balance control based on dual active bridge DC/DC converters in a power electronic traction transformer," *IEEE Trans. Power Electron.*, vol. 33, no. 2, pp. 1696–1714, Feb. 2018.

[2] J. Feng, W. Q. Chu, Z. Zhang, and Z. Q. Zhu, "Power electronic transformer-based railway traction systems: Challenges and opportunities," *IEEE J. Emerg. Sel. Topics Power Electron.*, vol. 5, no. 3, pp. 1237–1253, Sep. 2017.

[3] D. Wang *et al.*, "A 10-kV/400-V 500-kVA electronic power transformer," *IEEE Trans. Ind. Electron.*, vol. 63, no. 11, pp. 6653–6663, Nov. 2016.

[4] F. An, W. Song, K. Yang, S. Yang, and L. Ma, "A simple power estimation with triple phase-shift control for the output parallel DAB DC-DC converters in power electronic traction transformer for railway locomotive application," *IEEE Trans. Transport. Electrific.*, vol. 5, no. 1, pp. 299–310, Mar. 2019.

[5] X. She, A. Q. Huang, T. Zhao, and G. Wang, "Coupling effect reduction of a voltage-balancing controller in single-phase cascaded multilevel converters," *IEEE Trans. Power Electron.*, vol. 27, no. 8, pp. 3530–3543, Aug. 2012.

[6] N. Zhao, J. Liu, Y. Ai, J. Yang, J. Zhang, and X. You, "Power-linked predictive control strategy for power electronic traction transformer," *IEEE Trans. Power Electron.*, vol. 35, no. 6, pp. 6559–6571, Jun. 2020.

[7] L. He, J. Xiong, H. Ouyang, P. Zhang, and K. Zhang, "High-performance indirect current control scheme for railway traction four-quadrant converters," *IEEE Trans. Ind. Electron.*, vol. 61, no. 12, pp. 6645–6654, Dec. 2014.

[8] P. A. Dahono, "New hysteresis current controller for single-phase full-bridge inverters," *IET Power Electron*, vol. 2, no. 6, pp. 585–594, Aug. 2009.

[9] Y. Su, X. Ge, D. Xie, and K. Wang, "An active disturbance rejection control-based voltage control strategy of single-phase cascaded H-bridge rectifiers," *IEEE Trans. Ind. Appl.*, vol. 56, no. 5, pp. 5182–5193, Sep. 2020.

[10] H. Hu, Y. Zhou, X. Li, and K. Lei, "Low-frequency oscillation in electric railway depot: A comprehensive review," *IEEE Trans. Power Electron.*, vol. 36, no. 1, pp. 295–314, Jan. 2021.

[11] C. Zhang, S. Yu, and X. Ge, "A stationary-frame current vector control strategy for single-phase PWM rectifier," *IEEE Trans. Veh. Technol.*, vol. 68, no. 3, pp. 2640–2651, Mar. 2019.

[12] V. Blahnik, T. Kosan, Z. Peroutka, and J. Talla, "Control of a single-phase cascaded H-bridge active rectifier under unbalanced load," *IEEE Trans. Power Electron.*, vol. 33, no. 6, pp. 5519–5527, Jun. 2018.

[13] D. Yang, N. Wu, L. Yin, and Z. Lu, "Natural frame control of single-phase cascaded H-bridge multilevel converter based on fictive-phases construction," *IEEE Trans. Ind. Electron.*, vol. 65, no. 5, pp. 3848–3857, May 2018.

[14] Q. Zhong, P. Nguyen, Z. Ma, and W. Sheng, "Self-synchronized synchronverters: Inverters without a dedicated synchronization unit," *IEEE Trans. Power Electron.*, vol. 29, no. 2, pp. 617–630, Feb. 2014.

[15] C. Qi, X. Chen, P. Tu, and P. Wang, "Cell-by-cell-based finite-control- set model predictive control for a single-phase cascaded H-bridge rectifier," *IEEE Trans. Power Electron.*, vol. 33, no. 2, pp. 1654–1665, Feb. 2018.

[16] W. Song, Z. Deng, S. Wang, and X. Feng, "A simple model predictive power control strategy for single-phase PWM converters with modulation function optimization," *IEEE Trans. Power Electron.*, vol. 31, no. 7, pp. 5279–5289, Jul. 2016.

[17] Y. Zhang, J. Jin, and L. Huang, "Model-free predictive current control of PMSM drives based on extended state observer using ultralocal model," *IEEE Trans. Ind. Electron.*, vol. 68, no. 2, pp. 993–1003, Feb. 2021.

[18] H. Iman-Eini, J. Schanen, S. Farhangi, and J. Roudet, "A modular strategy for control and voltage balancing of cascaded H-bridge rectifiers," *IEEE Trans. Power Electron.*, vol. 23, no. 5, pp. 2428–2442, Sep. 2008.

[19] X. She, A. Q. Huang, and G. Wang, "3-D space modulation with voltage balancing capability for a cascaded seven-level converter in a solid-state transformer," *IEEE Trans. Power Electron.*, vol. 26, no. 12, pp. 3778–3789, Dec. 2011.

[20] J. I. Leon, S. Vazquez, A. J. Watson, L. G. Franquelo, P. W. Wheeler, and J. M. Carrasco, "Feed-forward space vector modulation for single-phase multilevel cascaded converters with any DC voltage ratio," *IEEE Trans. Ind. Electron.*, vol. 56, no. 2, pp. 315–325, Feb. 2009.

[21] C. Wang, Y. Zhuang, J. Jiao, H. Zhang, C. Wang, and H. Cheng, "Topologies and control strategies of cascaded bridgeless multilevel rectifiers," *IEEE J. Emerg. Sel. Topics Power Electron.*, vol. 5, no. 1, pp. 432–444, Mar. 2017.

[22] T. Zhao, G. Wang, S. Bhattacharya, and A. Q. Huang, "Voltage and power balance control for a cascaded H-bridge converter-based solid-state transformer," *IEEE Trans. Power Electron.*, vol. 28, no. 4, pp. 1523–1532, Apr. 2013.

[23] B. Liu, W. Song, Y. Li, and B. Zhan, "Performance improvement of DC capacitor voltage balancing control for cascaded H-bridge multilevel converters," *IEEE Trans. Power Electron.*, vol. 36, no. 3, pp. 3354–3366, Mar. 2021.

[24] J. Ma, W. Song, S. Wang, and X. Feng, "Model predictive direct power control for single-phase three-level rectifier at low switching frequency," *IEEE Trans. Power Electron.*, vol. 33, no. 2, pp. 1050–1062, Feb. 2018.

[25] B. Liu, W. Song, J. Ma, and X. Feng, "Dynamic performance improvement of single-phase PWM converters with power hysteresis control scheme," *IET Power Electron.*, vol. 11, no. 12, pp. 1894–1902, Oct. 2018.

[26] B. Bahrani, A. Rufer, S. Kenzelmann, and L. A. C. Lopes, "Vector control of single-phase voltage-source converters based on fictive-axis emulation," *IEEE Trans. Ind. Appl.*, vol. 47, no. 2, pp. 831–840, Mar. 2011.

[27] C. E. Garcia and M. Morari, "Internal model control. a unifying review and some new results," *Ind. Eng. Chem. Proc. Des. Develop.*, vol. 21, no. 2, pp. 308–323, Apr. 1982.

[28] C. Xia, Y. Yan, P. Song, and T. Shi, "Voltage disturbance rejection for matrix converter-based PMSM drive system using internal model control," *IEEE Trans. Ind. Electron.*, vol. 59, no. 1, pp. 361–372, Jan. 2012.

[29] H. R. Ossareh, S. Wisotzki, J. Buckland Seeds, and M. Jankovic, "An internal model control-based approach for characterization and controller tuning of turbocharged gasoline engines," *IEEE Trans. Control Syst. Technol.*, vol. 29, no. 2, pp. 866–875, Mar. 2021.
[30] Z. Yin, C. Bai, N. Du, C. Du, and J. Liu, "Research on internal model control of induction motors based on luenberger disturbance observer," *IEEE Trans. Power Electron.*, vol. 36, no. 7, pp. 8155–8170, Jul. 2021.
[31] J. Huang, Z. Zhang, J. Han, and W. Jiang, "Dynamic performance improvement for permanent magnet generator system using current compensating method with two-degrees-of-freedom control," *IEEE Trans. Ind. Electron.*, vol. 68, no. 4, pp. 2823–2833, Apr. 2021.
[32] R. Zhang, Z. Yin, N. Du, J. Liu, and X. Tong, "Robust adaptive current control of a 1.2-MW direct-drive PMSM for traction drives based on internal model control with disturbance observer," *IEEE Trans. Transport. Electrific.*, vol. 7, no. 3, pp. 1466–1481, Sep. 2021.
[33] Z. Zheng, Z. Gao, C. Gu, L. Xu, K. Wang, and Y. Li, "Stability and voltage balance control of a modular converter with multiwinding high-frequency transformer," *IEEE Trans. Power Electron.*, vol. 29, no. 8, pp. 4183–4194, Aug. 2014.
[34] A. Kulkarni and V. John, "A novel design method for SOGI-PLL for minimum settling time and low unit vector distortion," in *Proc. IEEE Ind. Electron. Soc. Annu. Conf.*, 2013, pp. 274–279.
[35] D. Xie, C. Lin, Q. Deng, X. Ge, and B. Gou, "A fast diagnosis scheme for multiple switch faults in cascaded H-bridge multilevel converters," *IEEE Trans. Transport. Electrific.*, vol. 7, no. 3, pp. 1000–1015, Sep. 2021.
[36] R. C. Dorf and R. H. Bishop, *Modern Control Systems*, 12th ed. Upper Saddle River, NJ, USA: Prentice-Hall, 2010.
[37] R. Cai, R. Zheng, M. Liu, and M. Li, "Robust control of PMSM using geometric model reduction and μ-synthesis," *IEEE Trans. Ind. Electron.*, vol. 65, no. 1, pp. 498–509, Jan. 2018.
[38] Y. Lei, K. Wang, L. Zhao, Q. Ge, Z. Li, and Y. Li, "An improved torque and current pulsation suppression method for railway traction drives under fluctuating DC-Link voltage," *IEEE Trans. Power Electron.*, vol. 33, no. 10, pp. 8565–8577, Oct. 2018.

Haoran Liu received the B.S. degree in electrical engineering and automation from Panzhihua University, Panzhihua, China, in 2015, and the M.S. degree in computer application technology from Central South University of Forestry and Technology, Changsha, China, in 2018. He is currently working toward the Ph.D. degree in electrical engineering with the School of Electrical Engineering, Southwest Jiaotong University, Chengdu, China.

His research interests include robust control and modulation of power converters in railway applications.

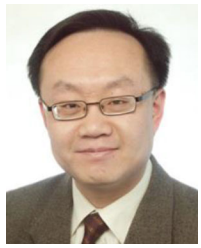

Lei Ma (Member, IEEE) received the B.Eng. degree in automatic control from Chongqing University, Chongqing, China, in 1993, the M.Sc. degree in electrical engineering from Southwest Jiaotong University, Chengdu, China, in 1996, and the Dr.-Ing. degree in electrical engineering from Ruhr University Bochum, Bochum, Germany, in 2006.

From 2006 to 2009, he was an Assistant Professor in robotics and telematics with the University of Würzburg, and also the Deputy Director and a Member of the Board of Supervisors with the Zentrum für Telematik e.V., Würzburg, Germany. Since September 2009, he has been a Professor with the School of Electrical Engineering, Southwest Jiaotong University, Chengdu, China.

His research interests include control theory with applications to robotics, renewable energy, and rail transit systems.

Wensheng Song (Member, IEEE) received the B.S. degree in electronic and information engineering and the Ph.D. degree in electrical engineering from Southwest Jiaotong University, Chengdu, China, in 2006 and 2011, respectively.

He is currently a Full Professor with the School of Electrical Engineering, Southwest Jiaotong University. From September 2009 to September 2010, he was a Visiting Scholar with the Department of Electrical Engineering and Computer Science, University of California, Irvine, CA, USA. From July 2015 to December 2015, he was a Visiting Scholar with the University of Alberta, Edmonton, AB, Canada. His current research interests include power electronics, motor drives, electrical ac–dc–ac railway traction drive systems, and multilevel converters.

Lin Peng received the B.S. degree in communication engineering from the University of Electronic Science and Technology of China, Chengdu, China, in 2006, and the M.Eng. degree in control engineering from Chongqing University, Chongqing, China, in 2011. He is currently working toward the Ph.D. degree in electrical engineering with Southwest Jiaotong University, Chengdu, China.

His research interests include modeling and control of power converters in railway traction drive systems.